Applied Mathematical Modelling 40 (2016) 5462–5481

Contents lists available at ScienceDirect

Applied Mathematical Modelling

journal homepage: www.elsevier.com/locate/apm

Stability of natural convection in a vertical dielectric couple stress fluid layer in the presence of a horizontal AC electric field

B.M. Shankar[a,*], Jai Kumar[b], I.S. Shivakumara[c]

[a] Department of Mathematics, PES University, Bangalore 560 085, India
[b] ISRO Satellite Centre, Bangalore 560 017, India
[c] Department of Mathematics, Bangalore University, Bangalore 560 056, India

ARTICLE INFO

Article history:
Received 17 July 2014
Revised 21 November 2015
Accepted 6 January 2016
Available online 15 January 2016

Keywords:
Couple stress fluid
Natural convection
AC electric field
Linear stability
Galerkin method

ABSTRACT

The combined effect of couple stresses and a uniform horizontal AC electric field on the stability of buoyancy-driven parallel shear flow of a vertical dielectric fluid between vertical surfaces maintained at constant but different temperatures is investigated. Applying linear stability theory, stability equations are derived and solved numerically using the Galerkin method with wave speed as the eigenvalue. The critical Grashof number G_c, the critical wave number a_c and the critical wave speed c_c are computed for wide ranges of couple stress parameter Λ_c, AC electric Rayleigh number R_{ea} and the Prandtl number Pr. Based on these parameters, the stability characteristics of the system are discussed in detail. The value of Prandtl number at which the transition from stationary to travelling-wave mode takes place is found to be independent of AC electric Rayleigh number even in the presence of couple stresses but increases significantly with increasing Λ_c. Moreover, the effect of increasing R_{ea} is to instill instability, while the couple stress parameter shows destabilizing effect in the stationary mode but it exhibits a dual behavior if the instability is via travelling-wave mode. The streamlines and isotherms presented demonstrate the development of complex dynamics at the critical state.

1. Introduction

It is believed that in many geophysical and astrophysical phenomena the fluid flows are maintained by buoyancy forces, but the role of these forces is generally strongly modified by co-existing shear, rotation of the system as a whole, processes at a free surface and so on. An interaction between buoyancy and shearing forces prevails in the study of natural convection of a viscous fluid in a vertical fluid layer whose walls are held at constant but different temperatures. In such a system, the base flow becomes unstable when the Grashof number exceeds certain critical value. The stability aspects of this classical problem for the Newtonian fluid flow are studied extensively [1–5]. One important observation made was that the parallel flow undergoes a transition to a stationary multicell flow pattern for values of Prandtl number, $Pr < 12.7$ when the Grashof number exceeds a critical value and this theoretically observed fact was confirmed experimentally by Vest and Arpaci [6].

* Corresponding author. Tel.: +91 9008225155.
E-mail address: shankarmahadev07@gmail.com, bmshankar@pes.edu (B.M. Shankar).

http://dx.doi.org/10.1016/j.apm.2016.01.005
S0307-904X(16)00008-1/

Nomenclature

a	vertical wave number
c	wave speed
c_r	phase velocity
c_i	growth rate
$D = d/dx$	differential operator
$\vec{E}$	root-mean-square value of the electric field
E_0	root-mean-square value of the electric field at $x=0$
$\vec{f_e}$	force of electrical origin
$\vec{g}$	acceleration due to gravity
$G = \alpha g \beta h^4/\nu^2$	Grashof number
h	thickness of the dielectric fluid layer
$\hat{i}$	unit vector in x-direction
$\hat{k}$	unit vector in z-direction
p	pressure
$P = p - 0.5\rho(\partial\varepsilon/\partial\rho)(\vec{E}\cdot\vec{E})$	modified pressure
$Pr = \nu/\kappa$	Prandtl number
$\vec{q} = (u, v, w)$	velocity vector
$R_{ea} = \gamma^2\varepsilon_0 E_0^2\beta^2 h^4/\mu\kappa$	AC electric Rayleigh number
t	time
T	temperature
T_1	temperature of the left boundary
T_2	temperature of the right boundary
V	root-mean-square value of the electric potential
V_1	electric potential of the left boundary
V_2	electric potential of the right boundary
W_b	basic velocity
(x, y, z)	Cartesian co-ordinates

Greek symbols

α	thermal expansion coefficient
γ	thermal expansion coefficient of dielectric constant
η	couple stress viscosity
ε	dielectric constant
ε_0	reference dielectric constant at T_0
κ	thermal diffusivity
σ	electrical conductivity of the fluid
$\Lambda_c = h\sqrt{\mu/\eta}$	couple stress parameter
μ	fluid viscosity
$\nu(=\mu/\rho_0)$	kinematic viscosity
$\psi(x, z, t)$	stream function
Ψ	amplitude of vertical component of perturbed stream function
ϕ	amplitude of perturbed electric potential
ρ	fluid density
ρ_e	free charge density
ρ_0	reference density at T_0
θ	amplitude of perturbed temperature

The stability of fluid flows under the influence of electric/magnetic field has also received equal importance in the literature. The magnetic field effects become dominant when the fluid is highly electrically conducting and stability of such fluid flows under the influence of magnetic field has been studied in the past (Takashima [7] and references therein). If the fluid is dielectric with low electrical conductivity then the electric forces play a major role rather than magnetic forces in driving the motion. Electrohydrodynamic (EHD) stability of channel flow has attracted much attention, particularly because of its use in the field of microfluidics. For instance, in many micro-electro-mechanical-systems (MEMS) devices, rapid mixing is highly desired and can be achieved by applying an electric field, as in the experiments of Moctar et al. [8], Glasgow et al. [9] and Lin et al. [10]. The instability mechanisms, including joule heating effect, electro-osmotic convection, ion-electromigration, and electric conductivity gradients, are usually well-controlled either to enhance mixing in biochemical reactors [11] or to avoid unstable convection occurring in sample separation devices such as field amplified sample stacking [12,13] and isoelectric focusing (IEF) techniques [14]. Moreover, EHD forces have also been used to simulate the earth's gravitational field

during convection experiments carried out during a space shuttle flight. In this application, combining a radial electric field with a temperature gradient between concentric spheres engenders polarization forces that mimic gravity. A brief discussion on the applications of EHD instability has been presented by Lin [15].

A considerable number of theoretical and numerical studies have been devoted to the interaction of electric field with fluids. The effect of horizontal AC electric field on the stability of a plane convective flow of a vertical dielectric fluid layer has been investigated for over a wide range of Prandtl numbers by Takashima and Hamabata [16]. They found that a transition from stationary to travelling-wave instability occurs at a certain value of *Pr* between 12.4 and 12.5, which was later supported by Chen and Pearlstein [17]. Fujimura [18] showed that the transition value of *Pr* is given by 12.45425644. Smorodin [19] investigated the instability of convective liquid dielectric flow in the alternating field of a vertical capacitor with boundaries heated to different temperatures. The EHD instability of a horizontal rotating fluid layer with a vertical electrical conductivity gradient is considered by Ruo et al. [20].

Copious literature available on the stability of natural convection in a vertical fluid layer is mainly concerned with Newtonian fluids. Nonetheless, the hypothesis of a Newtonian fluid will be too restrictive and cannot precisely describe the characteristics of the fluid flow involved in many practical problems. Therefore, it is warranted to investigate the stability of natural convection for non-Newtonian fluids. As there exist different types of non-Newtonian fluids, it is not possible to discuss them together and each type of fluid has to be treated separately. Studies have been undertaken in the past to analyze the stability of non-Newtonian fluids, but the investigations carried out are limited to viscoelastic fluids; a type of non-Newtonian fluid (Frigaard et al. [21], Gozum and Arpaci [22], Takashima [23]).

There is another class of non-Newtonian fluids known as polar fluids which have received wider attention in recent years. In this connection, Eringen [24] and Stokes [25] developed separate theories referred to as micropolar fluid theory and couple stress fluid theory. The couple-stress fluid theory given by Stokes [25] represents the simplest generalization of the classical viscous fluid theory that allows for polar effects in which the order of differential equations is higher than the Navier–Stokes equations. The couple stress fluid theory is found to be important in a number of processes that occur in industry, such as the extrusion of polymer fluids, solidification of liquid crystals, cooling of metallic plates in a bath, exotic lubricants and colloidal fluids, liquids containing long-chain molecules as polymeric suspensions, electro-rheological fluids and so on.

Majority of the investigations are concerned with buoyancy driven convection in a horizontal couple stress fluid layer [26–30]. Recently, Shivakumara et al. [31] presented the effect of velocity and temperature boundary conditions on electrothermal convection in a rotating dielectric fluid layer considering the variation in the dielectric constant with the non-homogeneous temperature gradient in the bulk flow. Besides, effect of couple stresses and a uniform AC electric field on convective instability has been studied by Shivakumara et al. [32]. The effects of couple stresses on the hydrodynamic stability of plane Poiseuille flow has been investigated by Jain and Stokes [33]. Rudraiah et al. [34] investigated EHD stability of couple stress fluid flow in a horizontal channel occupied by a porous medium using energy method. Shankar et al. [35] used classical linear stability theory to examine the stability of natural convection in a vertical couple stress fluid layer, while the effect of horizontal AC electric field on the stability of natural convection in a vertical dielectric Newtonian fluid-saturated porous layer was studied recently by Shankar et al. [36].

Clearly, while much has been comprehended regarding the stability of couple stress fluid flow driven by combined shear and/or buoyancy forces, our understanding of electro-thermo-hydrodynamic (ETHD) instability of dielectric fluid flows most commonly encountered in practical situations as propounded earlier is far from complete. The seriousness of this deficiency is accentuated by the fact that ETHD instability is essentially important in the investigation of deleterious convection in IFE techniques and also in many engineering applications [15]. Besides, heat transfer by means of thermal convection may not meet the requirements in most of the practical situations particularly in MEMS. In such circumstances, EHD enhanced heat transfer emerges as an important alternative method to enhance heat transfer. The intent of the present work is to develop an appropriate mathematical model to investigate the stability of natural convection in a vertical dielectric couple stress fluid layer under the influence of uniform horizontal AC electric field. The side walls of the fluid layer are maintained at constant but different temperatures and as a result there exists variation in the dielectric constant which eventually causes ETHD instability by the dielectrophoretic force acting in the bulk of the fluid. From the mathematical view point, the effect of electric field adds one more equation for electric potential through Maxwell's equations and thereby the order of the stability equations increases by two. The resulting eigenvalue problem is solved numerically using the Galerkin method. The results for various values of Prandtl number, AC electric Rayleigh number and couple stress parameter are analyzed and some novelty regarding the transition region due to the presence of AC electric field and couple stresses is discussed in detail.

2. Problem formulation and the basic state

Fig. 1 shows the physical configuration of the problem considered. It consists of a vertical dielectric couple stress fluid layer whose vertical wall at $x = -h$ is prescribed at a uniform temperature T_1 and fixed electric potential $V_1 (= 0)$, while the wall at $x = h$ is maintained at uniform temperature $T_2 (> T_1)$ and at an alternating (60 Hz) potential whose root-mean-square value is V_2. A Cartesian coordinate system (x, y, z) is chosen with the origin in the middle of the fluid layer. The x-axis is horizontal and taken perpendicular to the plates while the z-axis is vertical and oriented upward. The gravity is acting in the negative z-direction. The basic equations consist of the balances of mass, linear momentum and energy along

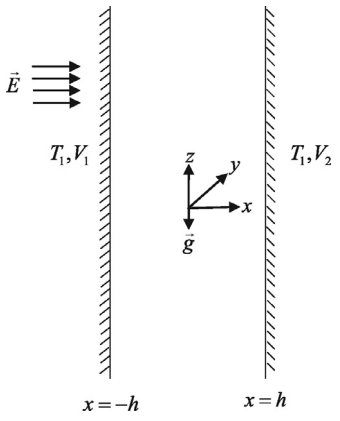

Fig. 1. Physical configuration.

with Maxwell equations. Under the Oberbeck–Boussinesq approximation and in the absence of body couples, the governing equations may be written as [16,25,32]

$$\nabla \cdot \vec{q} = 0, \tag{1}$$

$$\rho_0 \left[\frac{\partial \vec{q}}{\partial t} + (\vec{q} \cdot \nabla)\vec{q} \right] = -\nabla p + \rho \vec{g} + \mu \nabla^2 \vec{q} - \eta \nabla^4 \vec{q} + \vec{f}_e, \tag{2}$$

$$\frac{\partial T}{\partial t} + (\vec{q} \cdot \nabla) T = \kappa \nabla^2 T, \tag{3}$$

$$\nabla \times \vec{E} = 0 \quad \text{or} \quad \vec{E} = -\nabla V, \tag{4}$$

$$\nabla \cdot (\varepsilon \vec{E}) = 0, \tag{5}$$

$$\rho = \rho_0 \{1 - \alpha (T - T_0)\}, \tag{6}$$

$$\varepsilon = \varepsilon_0 [1 - \gamma (T - T_0)]. \tag{7}$$

In the above equations, $\vec{q} = (u, v, w)$ is the velocity vector, T is the temperature, p is the pressure, ρ is the fluid density, κ is the thermal diffusivity, μ is the fluid viscosity, η is the couple stress viscosity, V is the electric potential, $\vec{g}$ is the acceleration due to gravity, α is the thermal expansion coefficient, ρ_0 is the density at reference temperature $T = T_0$, ε is the dielectric constant, γ (> 0) is the thermal expansion coefficient of dielectric constant, $\vec{E}$ is the root-mean-square value of the electric field and $\vec{f}_e$ is the force of electrical origin which can be expressed as (Landau and Lifshitz [37])

$$\vec{f}_e = \rho_e \vec{E} - \frac{1}{2}(\vec{E} \cdot \vec{E}) \nabla \varepsilon + \frac{1}{2} \nabla \left(\rho \frac{\partial \varepsilon}{\partial \rho} \vec{E} \cdot \vec{E} \right), \tag{8}$$

where ρ_e is the free charge density. The fourth term on the right hand side of Eq. (2) is due to the presence of couple stresses and as a result the order of the differential equation is increased by two when compared to the Navier–Stokes equation ($\eta = 0$). The dielectric constant is assumed to be small and, for example, for water $\gamma = 2.14 \times 10^{-3}\,\mathrm{K}^{-1}$ and $\varepsilon_0 = 7.0833 \times 10^{-10}\,\mathrm{F\,m}^{-1}$.

In the basic state, the flow is considered to be fully developed steady laminar and unidirectional. Thus,

$$\vec{q} = W_b(x)\hat{k}, \quad P = P_b(x, z), \quad \vec{E} = \vec{E}_b(x)\hat{i}, \quad T = T_b(x), \quad \rho = \rho_b(x), \quad \varepsilon = \varepsilon_b(x), \quad V = V_b(x), \tag{9}$$

where $P = p - 0.5\rho(\partial\varepsilon/\partial\rho)(\vec{E} \cdot \vec{E})$ is the modified pressure and the subscript b denotes the basic state. The solution for the basic state can readily be obtained and found to be

$$W_b = \frac{\alpha g \beta}{12 \mu \nu} \left[x\{(h^2 - x^2)\mu - 6\eta\} + 6h\eta \,\mathrm{cosech}\left(h\sqrt{\frac{\mu}{\eta}} \right) \sinh\left(x\sqrt{\frac{\mu}{\eta}} \right) \right], \tag{10}$$

$$P_b = \text{const} - \rho_0 g z + \frac{\varepsilon_0 E_0^2}{2(1 - \gamma \beta x)}, \tag{11}$$

$$T_b - T_0 = \beta x/2; \quad \beta = \Delta T/h, \tag{12}$$

$$\rho_b = \rho_0 \left(1 - \frac{\alpha \beta x}{2} \right), \tag{13}$$

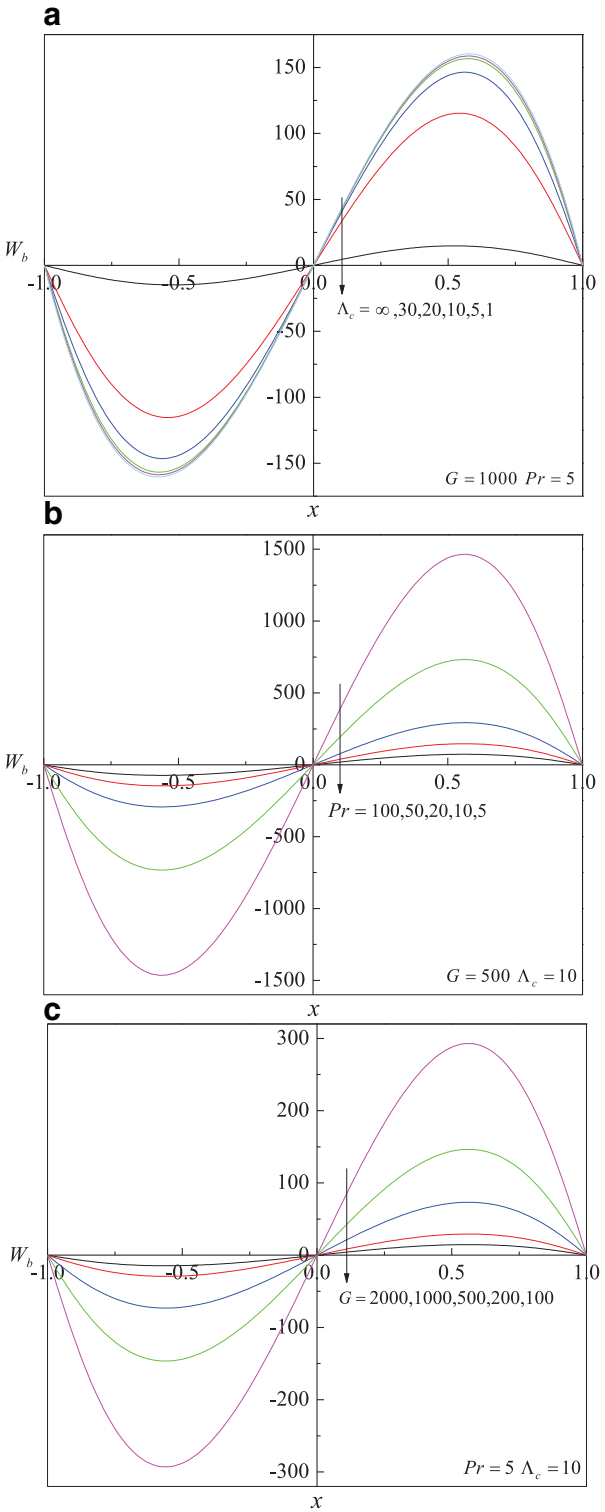

Fig. 2. Velocity profiles of the base flow.

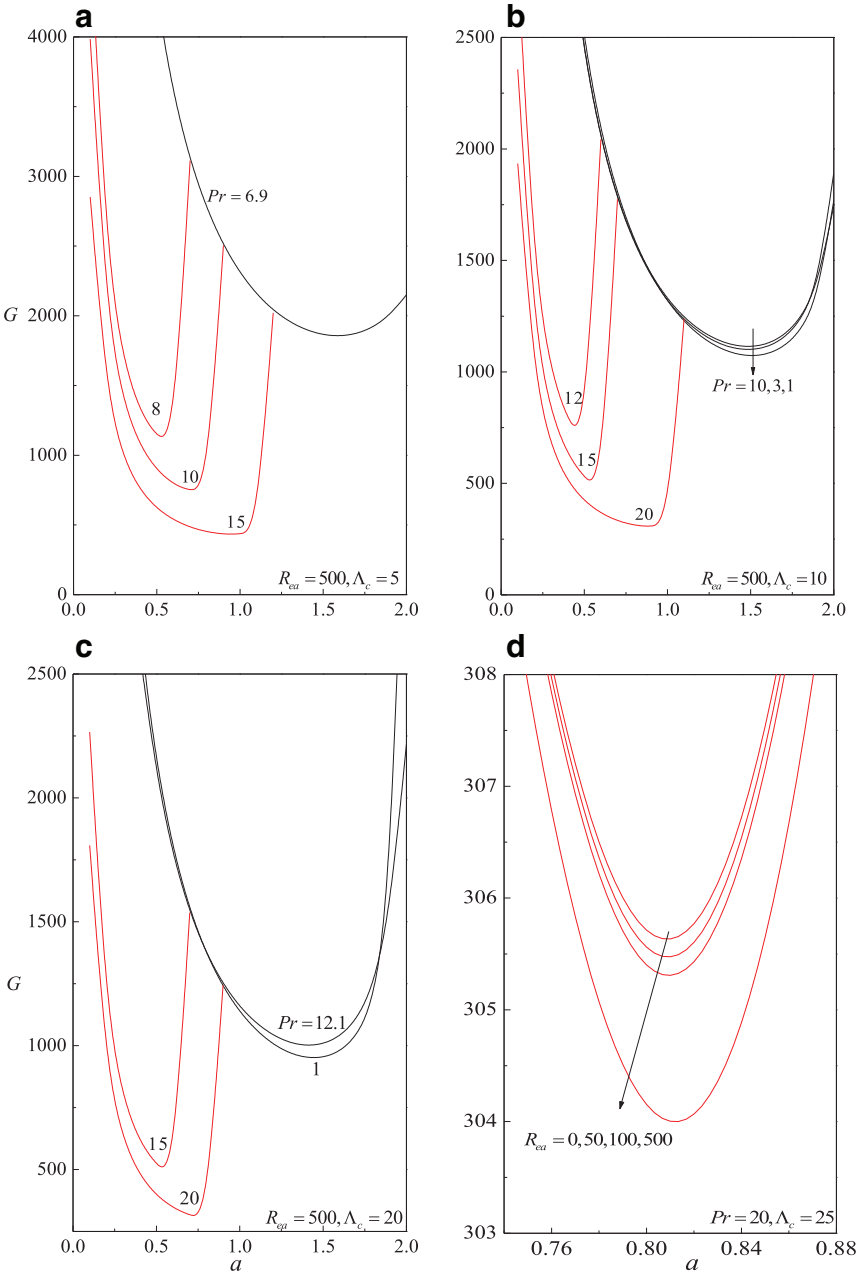

Fig. 3. Neutral stability curves. (——) Stationary modes and (——) travelling-wave modes.

$$\varepsilon_b = \varepsilon_0\left(1 - \frac{\gamma\beta x}{2}\right), \tag{14}$$

$$\vec{E}_b = \frac{E_0}{1 - \gamma\beta x/2}\hat{i}, \tag{15}$$

and hence

$$V_b = \frac{2E_0}{\gamma\beta}\log\left(\frac{1 - \gamma\beta x/2}{1 + \gamma\beta h/2}\right), \tag{16}$$

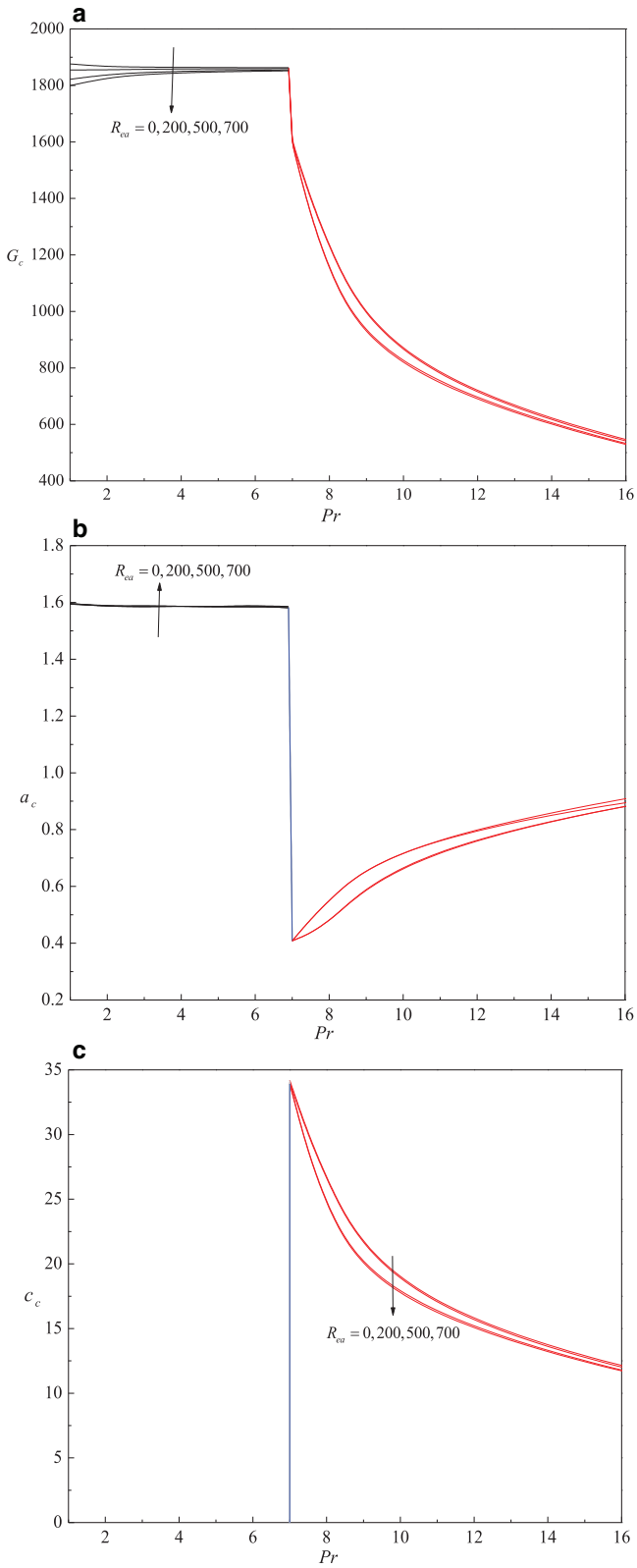

Fig. 4. Variation of (a) critical Grashof number G_c, (b) critical wave number a_c and (c) critical wave speed c_c with the Prandtl number Pr for a fixed value of $\Lambda_c(= 5)$ and for various values of the AC electric Rayleigh number R_{ea}. (——) Stationary modes, (——) travelling-wave modes and (——) transition modes.

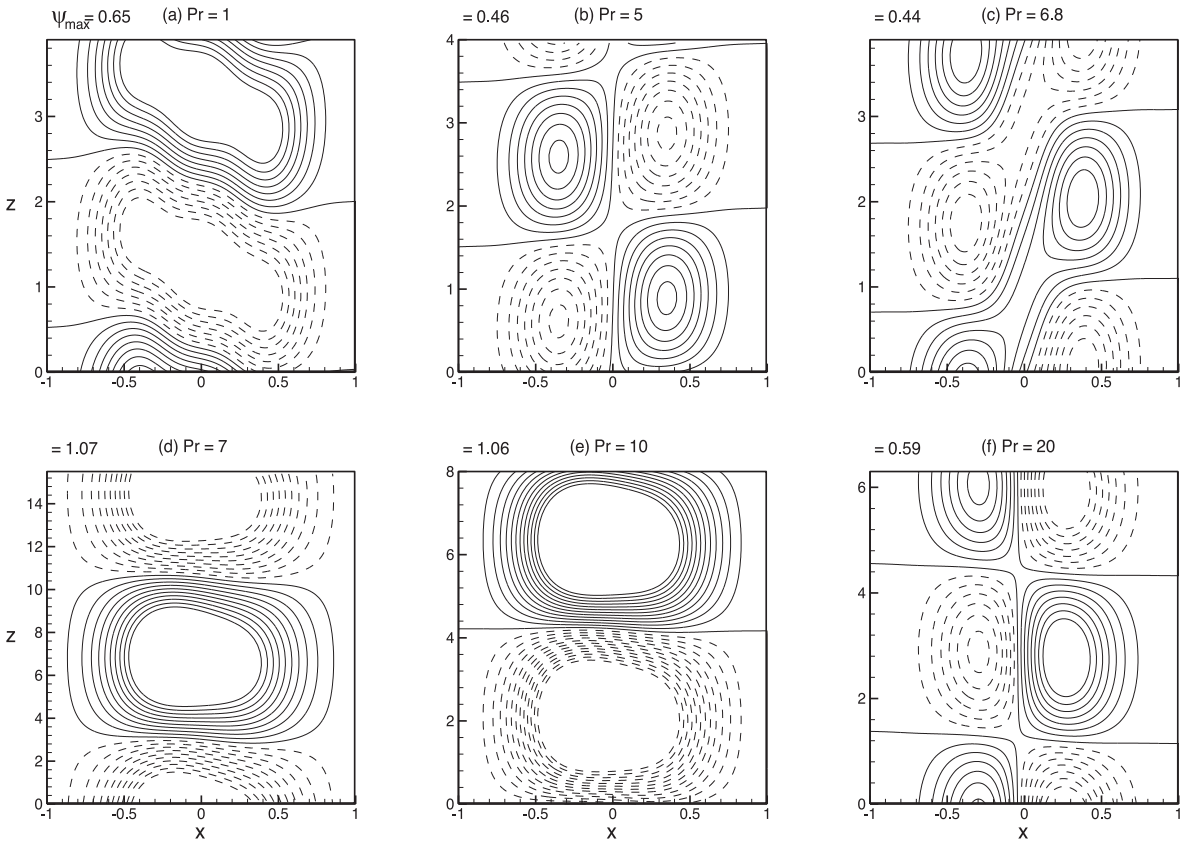

Fig. 5. Pattern variation of streamlines for different values of *Pr* when $\Lambda_c = 5$ and $R_{ea} = 200$.

where

$$E_0 = \frac{\gamma\beta V_2}{2}\log\left(\frac{1+\gamma\beta h/2}{1-\gamma\beta h/2}\right) \tag{17}$$

is the root-mean-square value of the electric field at $x = 0$ and $\nu(=\mu/\rho_0)$ is the kinematic viscosity. It is to be noted that in the basic state the electric field does not affect the flow field.

3. Perturbed state and the linear stability equations

Small disturbances of arbitrary form are superimposed upon the basic state in the following manner:

$$\vec{q} = \vec{q}_b + \vec{q}', \quad P = P_b(x,z) + P', \quad V = V_b + V', \quad T = T_b + T', \quad \rho = \rho_b + \rho', \quad \varepsilon = \varepsilon_b + \varepsilon', \tag{18}$$

where $\vec{q}'$, P', V', T', ρ' and ε' are perturbations over their equilibrium counterparts. Substituting Eq. (18) into Eqs. (1)–(3), linearizing by neglecting the product of primed quantities, we get

$$\nabla\cdot\vec{q}' = 0, \tag{19}$$

$$\frac{\partial\vec{q}'}{\partial t} + (\vec{q}_b\cdot\nabla)\vec{q}' + (\vec{q}'\cdot\nabla)\vec{q}_b = -\frac{1}{\rho_0}\nabla P' + \nu\nabla^2\vec{q}' - \frac{\eta}{\rho_0}\nabla^4\vec{q}' - \frac{E_0\gamma\beta\varepsilon_0}{2\rho_0}\frac{\partial V'}{\partial x}\hat{i} - \frac{E_0^2\gamma^2\beta\varepsilon_0}{2\rho_0}T'\hat{i} + \alpha T' g\hat{k}, \tag{20}$$

$$\frac{\partial T'}{\partial t} + (\vec{q}_b\cdot\nabla)\vec{q}' + (\vec{q}'\cdot\nabla)T_b = \kappa\nabla^2 T', \tag{21}$$

$$\gamma E_0\frac{\partial T'}{\partial x} = -\nabla^2 V'. \tag{22}$$

It may be noted that the presence of AC electric field introduces an additional stability equation of order 2 given by Eq. (22). We restrict our attention to two-dimensional disturbances (Squire's theorem [38] provides justification for working

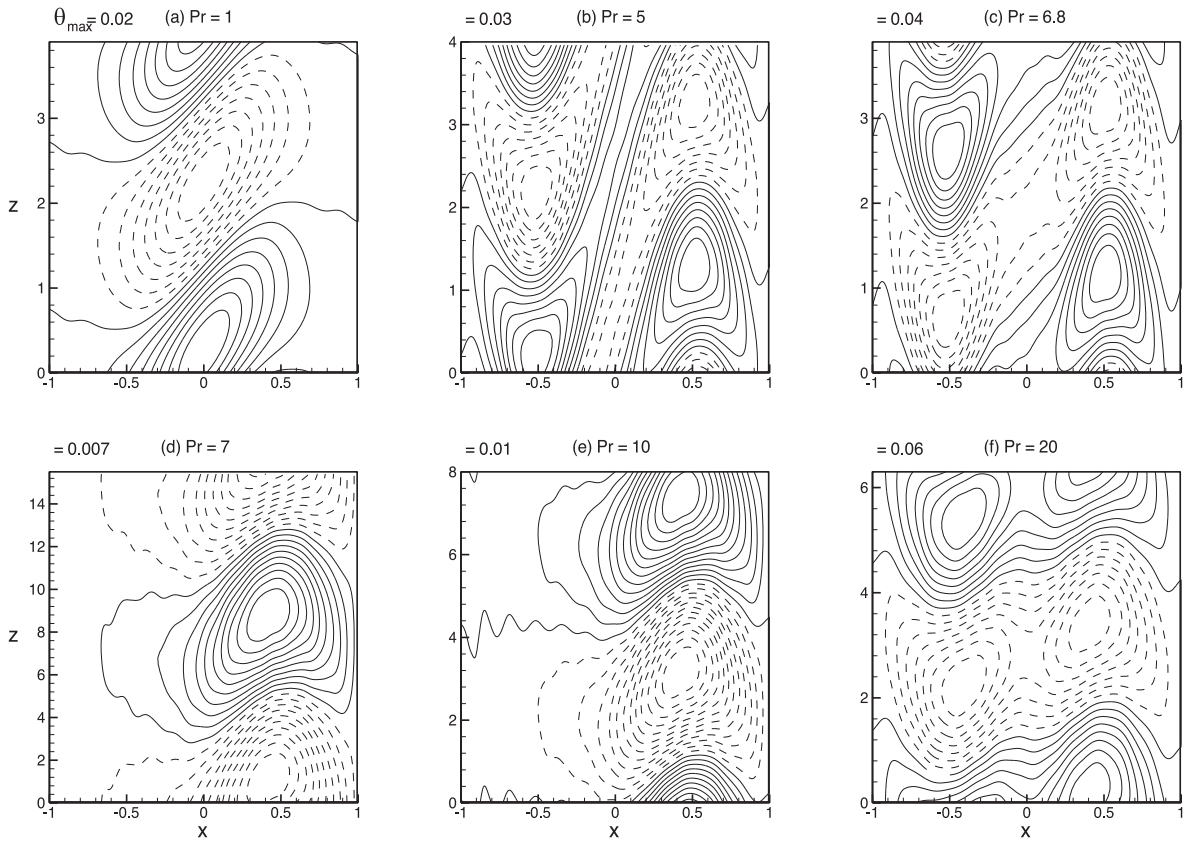

Fig. 6. Pattern variation of isotherms for different values of Pr when $\Lambda_c = 5$ and $R_{ea} = 200$.

in two dimensions rather than three dimensions) and the resulting equations are made dimensionless by scaling (x, y, z) by h, t by h^2/ν, $\vec{q}'$ by κ/h, T' by βh, V' by $\gamma\beta E_0 h^2$ and P' by $\rho_0\kappa\nu/h^2$ to get (after discarding the primes for simplicity)

$$\frac{\partial u}{\partial x} + \frac{\partial w}{\partial z} = 0, \tag{23}$$

$$\frac{\partial u}{\partial t} + \frac{W_b}{Pr}\frac{\partial u}{\partial z} = -\frac{\partial P}{\partial x} + \left(\frac{\partial^2 u}{\partial x^2} + \frac{\partial^2 u}{\partial z^2}\right) - \frac{1}{\Lambda_c^2}\left(\frac{\partial^4 u}{\partial x^4} + \frac{\partial^4 u}{\partial z^4} + 2\frac{\partial^4 u}{\partial x^2 \partial z^2}\right) - \frac{R_{ea}}{2}\left(\frac{\partial V}{\partial x} + T\right), \tag{24}$$

$$\frac{\partial w}{\partial t} + \frac{1}{Pr}\left(u\,DW_b + W_b\frac{\partial w}{\partial z}\right) = -\frac{\partial P}{\partial z} + \left(\frac{\partial^2 w}{\partial x^2} + \frac{\partial^2 w}{\partial z^2}\right) - \frac{1}{\Lambda_c^2}\left(\frac{\partial^4 w}{\partial x^4} + \frac{\partial^4 w}{\partial z^4} + 2\frac{\partial^4 w}{\partial x^2 \partial z^2}\right) + GPrT, \tag{25}$$

$$\frac{\partial T}{\partial t} + \frac{1}{Pr}\left(W_b\frac{\partial T}{\partial z} + \frac{u}{2}\right) = \frac{1}{Pr}\left(\frac{\partial^2 T}{\partial x^2} + \frac{\partial^2 T}{\partial z^2}\right), \tag{26}$$

$$\frac{\partial T}{\partial x} = -\left(\frac{\partial^2 V}{\partial x^2} + \frac{\partial^2 V}{\partial z^2}\right), \tag{27}$$

where $D = d/dx$, $R_{ea} = \gamma^2\varepsilon_0 E_0^2\beta^2 h^4/\mu\kappa$ is the AC electric Rayleigh number, $Pr = \nu/\kappa$ is the Prandtl number, $G = \alpha g\beta h^4/\nu^2$ is the Grashof number and $\Lambda_c = h\sqrt{\mu/\eta}$ is the couple stress parameter. The basic velocity W_b is in the dimensionless form now and given by

$$W_b = -\frac{G\,Pr}{12\Lambda_c^2}\left[x\left\{6 + \Lambda_c^2(-1 + x^2)\right\} - 6\,\mathrm{cosech}(\Lambda_c)\sinh(\Lambda_c x)\right]. \tag{28}$$

The effect of Λ_c, Pr and G on the basic flow W_b is demonstrated in Fig. 2. We eliminate the pressure term P from the momentum equations, introduce a stream function $\psi(x, z, t)$ through

$$u = \frac{\partial \psi}{\partial z},$$

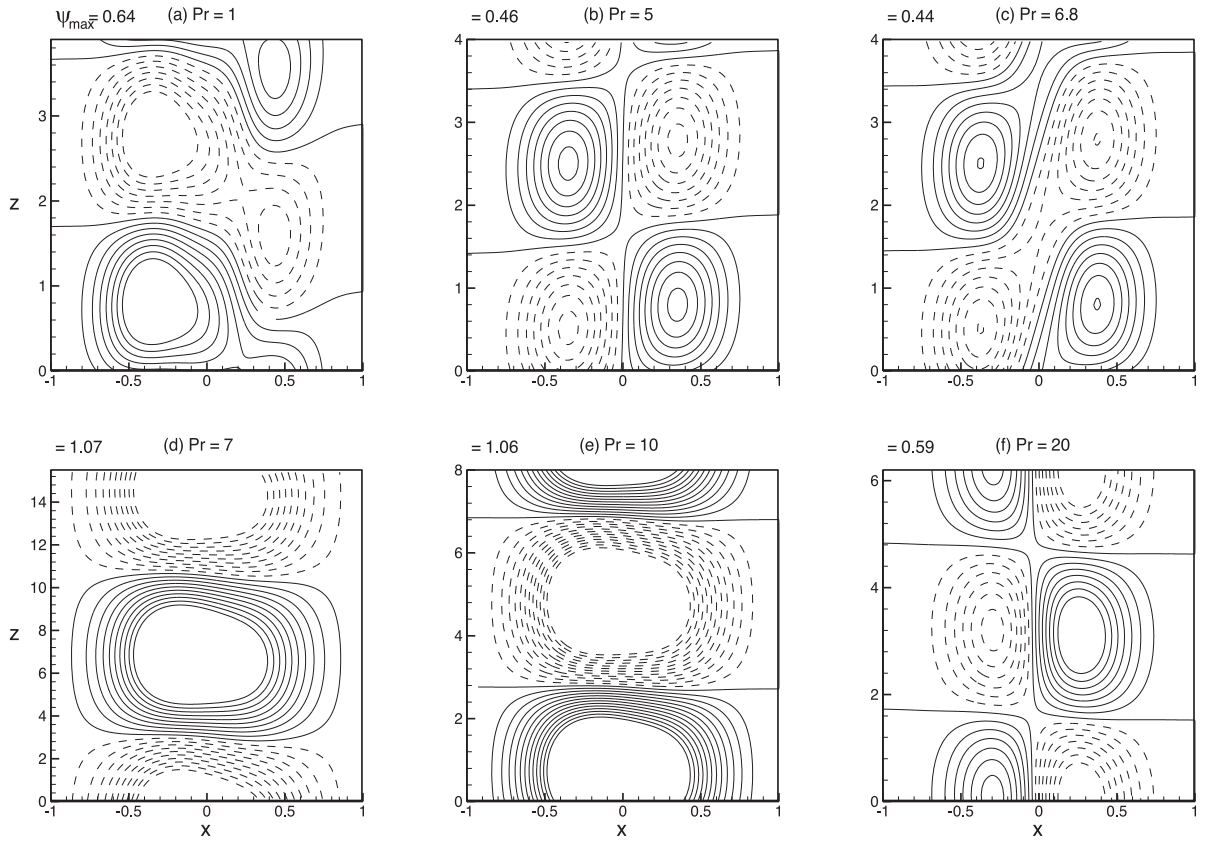

Fig. 7. Pattern variation of streamlines for different values of Pr when $\Lambda_c = 5$ and $R_{ea} = 500$.

$$w = -\frac{\partial \psi}{\partial x}, \tag{29}$$

and seek normal mode solution of the form

$$\{\psi, T, V\} = \{\Psi, \theta, \phi\}(x) e^{ia(z-ct)}, \tag{30}$$

where c is the wave speed and a is the vertical wave number which is real and positive. The resulting governing equations then take the form

$$\left(\frac{W_b}{Pr} - c\right)(D^2 - a^2)\Psi - \frac{1}{Pr} D^2 W_B \Psi + \frac{R_{ea}}{2}(D\phi + \theta) = \frac{1}{ia}\left[(D^2 - a^2)^2 \Psi - \frac{1}{\Lambda_c^2}(D^2 - a^2)^3 \Psi - GPrD\theta\right], \tag{31}$$

$$\left(\frac{W_b}{Pr} - c\right)\theta + \frac{1}{2Pr}\Psi = \frac{1}{iaPr}(D^2 - a^2)\theta, \tag{32}$$

$$D\theta + (D^2 - a^2)\phi = 0. \tag{33}$$

In general, $c = c_r + ic_i$, where c_r is the phase velocity and c_i is the growth rate.

It is considered that the vertical boundaries of the dielectric couple stress fluid are rigid, isothermal and the tangential electric field vanishes. Thus the associated boundary conditions are

$$\Psi = D\Psi = D^3\Psi = \theta = \phi = 0 \text{ at } x = \pm 1. \tag{34}$$

4. Method of solution

The eigenvalue problem constituted by Eqs. (31)–(33) together with the boundary conditions (34) is solved numerically using the Galerkin method. Accordingly, $\Psi(x)$, $\theta(x)$ and $\phi(x)$ are expanded in terms of Legendre polynomials in the form

$$\Psi(x) = \sum_{n=0}^{N} a_n \xi_n(x), \quad \theta(x) = \sum_{n=0}^{N} b_n \zeta_n(x), \quad \phi(x) = \sum_{n=0}^{N} c_n \zeta_n(x) \tag{35}$$

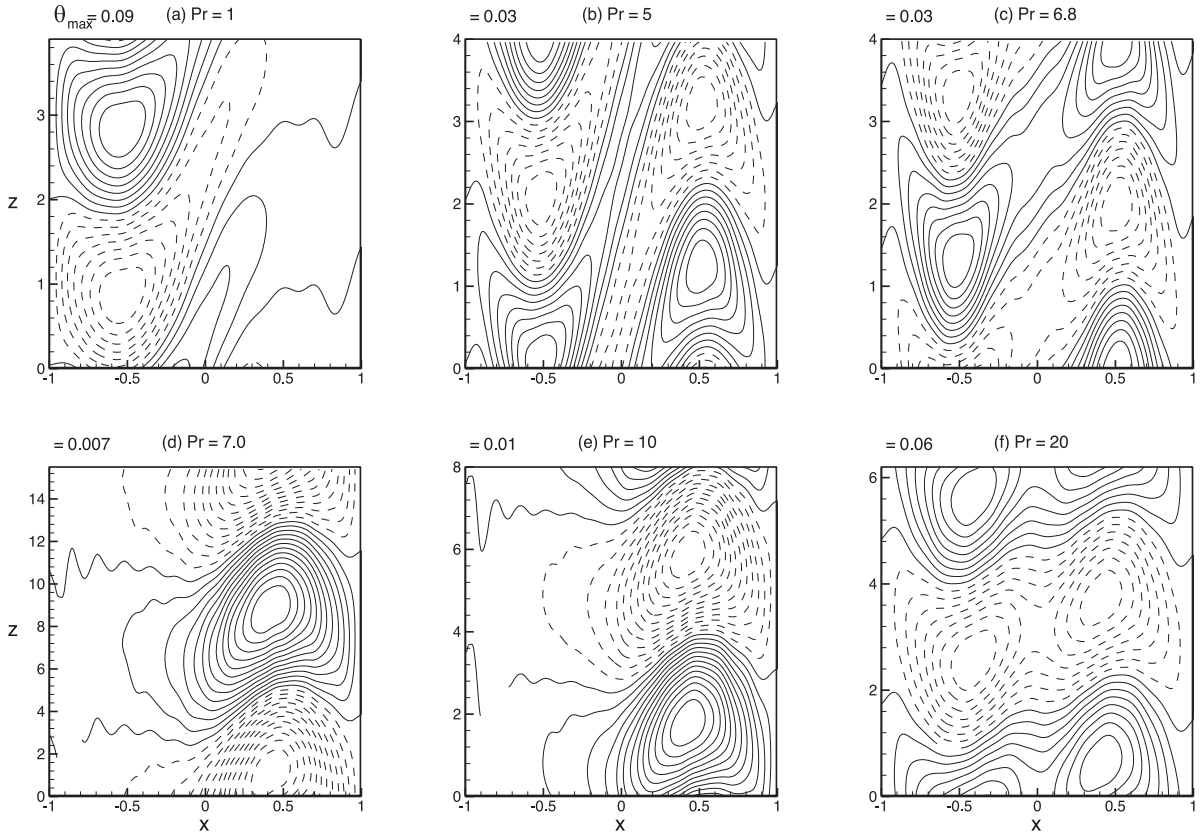

Fig. 8. Pattern variation of isotherms for different values of *Pr* when $\Lambda_c = 5$ and $R_{ea} = 500$.

with the corresponding base functions

$$\xi_n(x) = (x^2-3)(x^2-1)^2 P_n(x), \quad \zeta_n(x) = (1-x^2)P_n(x). \tag{36}$$

$P_n(x)$ is the Legendre polynomial of degree n and a_n, b_n, and c_n are constants. It may be noted that $\Psi(x), \theta(x)$, and $\phi(x)$ satisfy the boundary conditions. Eq. (35) is substituted into Eqs. (31)–(33) and the resulting error is required to be orthogonal to $\xi_m(x)$ and $\zeta_m(x)$ for $m = 0, 1, 2, \ldots N$. This gives

$$\begin{aligned}
&\frac{Pr}{\Lambda_c^2}\sum_{n=0}^{N} a_n \int_{-1}^{1} \left(\xi_n''' \xi_m''' + 3a^2 \xi''_n \xi''_m + 3a^4 \xi'_n \xi'_m + a^6 \xi_n \xi_m\right) dx \\
&\quad + Pr \sum_{n=0}^{N} a_n \int_{-1}^{1} (\xi_n'' \xi_m'' + 2a^2 \xi_n' \xi_m' + a^4 \xi_n \xi_m) dx \\
&\quad + ia \sum_{n=0}^{N} a_n \int_{-1}^{1} \left\{ \left(\frac{d^2 W_b}{dx^2} + a^2 W_b \right) \xi_n \xi_m - W_b \xi_n'' \xi_m \right\} dx - G\,Pr^2 \sum_{n=0}^{N} b_n \int_{-1}^{1} \zeta_n' \xi_m dx \\
&\quad - \frac{ia Pr\, R_{ea}}{2} \left(\sum_{n=0}^{N} b_n \int_{-1}^{1} \zeta_n \xi_m dx + \sum_{n=0}^{N} c_n \int_{-1}^{1} \zeta_n' \xi_m dx \right) \\
&= iac\, Pr \sum_{n=0}^{N} a_n \int_{-1}^{1} (\xi'_n \xi'_m + a^2 \xi_n \xi_m) dx,
\end{aligned} \tag{37}$$

$$\frac{ia}{2}\sum_{n=0}^{N} a_n \int_{-1}^{1} \xi_n \zeta_m\, dx + ia \sum_{n=0}^{N} b_n \int_{-1}^{1} W_b\, \zeta_n \zeta_m\, dx + \sum_{n=0}^{N} b_n \int_{-1}^{1} (\zeta'_n \zeta'_m + a^2 \zeta_n \zeta_m)\, dx = iac\, Pr \sum_{n=0}^{N} b_n \int_{-1}^{1} \zeta_n \zeta_m\, dx, \tag{38}$$

$$-\sum_{n=0}^{N} b_n \int_{-1}^{1} \zeta'_n \zeta_m\, dx + \sum_{n=0}^{N} c_n \int_{-1}^{1} (\zeta'_n \zeta'_m + a^2 \zeta_n \zeta_m)\, dx = 0 \tag{39}$$

in which the primed quantities denote differentiation with respect to *x*.

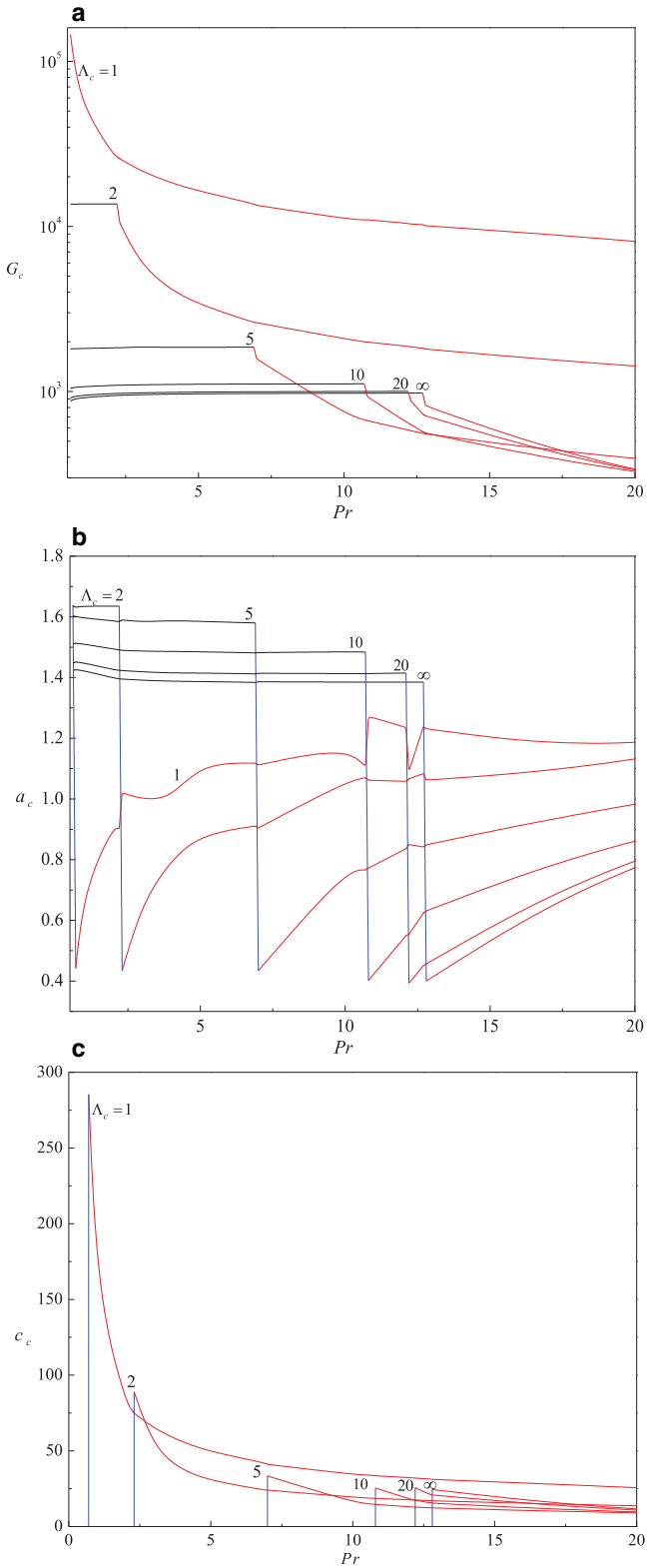

Fig. 9. Variation of (a) critical Grashof number G_c, (b) critical wave number a_c and (c) critical wave speed c_c with the Prandtl number Pr for a fixed value of the AC electric Rayleigh number R_{ea}(=500) and for various values of Λ_c. (——) Stationary modes, (——) travelling-wave modes and (——) transition modes.

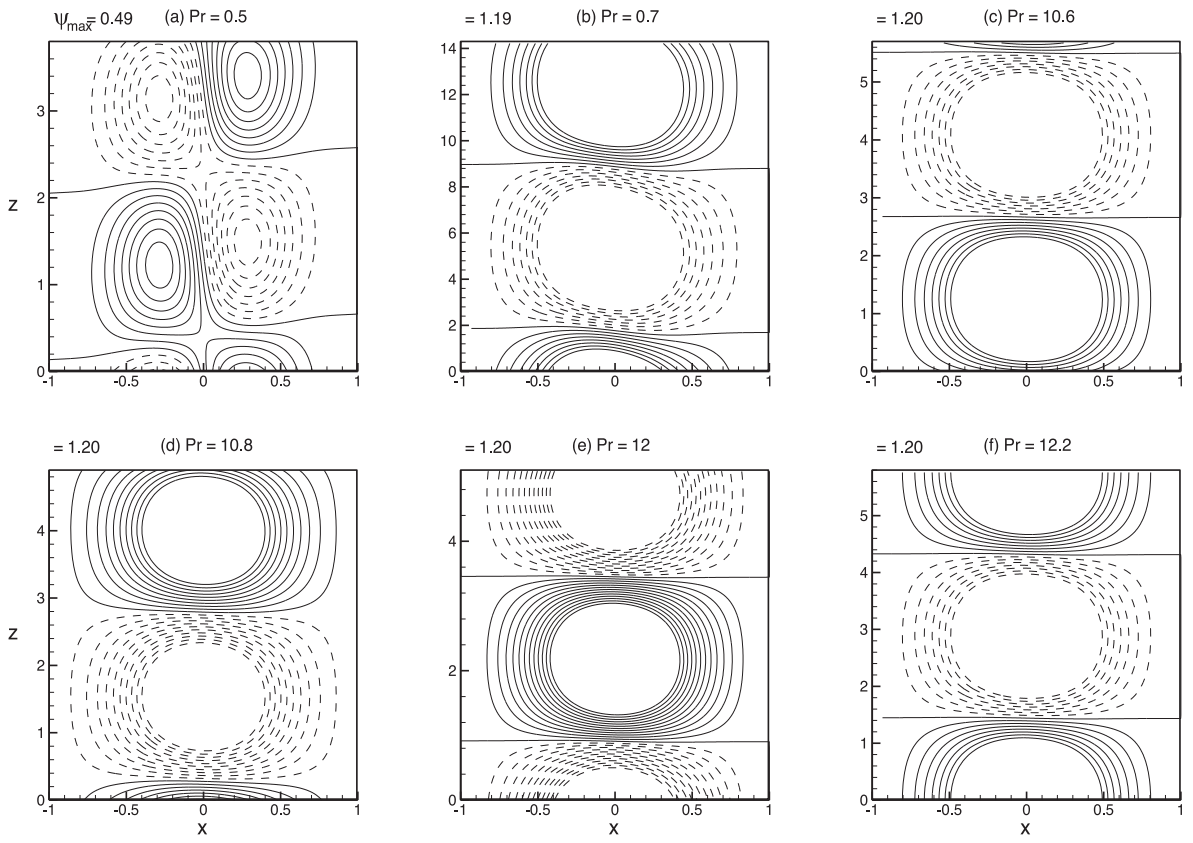

Fig. 10. Pattern variation of streamlines for different values of *Pr* when $\Lambda_c = 1$ and $R_{ea} = 500$.

The above equations form the following system of linear algebraic equations:

$$AX = cBX \tag{40}$$

where A and B are complex matrices, c is the eigenvalue and X is the eigenvector. To solve the above generalized eigenvalue problem, the DGVLCG of IMSL library [39] is employed. The routine is based on the QZ algorithm (Molar and Stewart [40]) which has the following four sections:

(i) Simultaneously reducing the matrix A to upper Heisenberg form ($a_{ij} = 0$ for $i > j + 1$) and reducing the matrix B to upper triangular form ($b_{ij} = 0$ for $i > j$).
(ii) Iteratively reducing A to quasi-triangular form while preserving the triangularity of B.
(iii) The determination of the eigenvalues from the quasi-triangular and triangular matrices.
(iv) The determination of the eigenvectors.

The critical wave speed c_c, the corresponding critical Grashof number G_c and the wave number a_c are determined for various values of Prandtl number *Pr*, AC electric Rayleigh number R_{ea} and the couple stress parameter Λ_c following the procedure outlined in Shankar et al. [41].

5. Results and discussion

A comprehensive numerical study on the stability of natural convection in a vertical dielectric couple stress fluid layer in the presence of a uniform horizontal AC electric field is presented. The critical Grashof number G_c and the critical wave speed c_c are computed with respect to the wave number a for various values of AC electric Rayleigh number R_{ea}, couple stress parameter Λ_c and the Prandtl number *Pr*using the Galerkin method. In most of the experiments, the depth over which the electric permittivity varies with temperature is generally in the order of millimeters and the kinematic viscosity and thermal diffusivity of the water-borne liquid used for biofluidics are about $\nu = 9.7 \times 10^{-7}\,\mathrm{m}^2/\mathrm{s}$ and $\kappa = 1.4 \times 10^{-7}\,\mathrm{m}^2/\mathrm{s}$, respectively. Thus the Prandtl number is approximately 7 and the other parameters are chosen in their admissible ranges to examine the instability characteristics of the system.

The convergence of the numerical method depends on the order of the base polynomial (N) as well as grid size (M) used to integrate the terms involved in Eqs. (37)–(39) (see Table 1). It can be seen from this table that for a fixed M, the

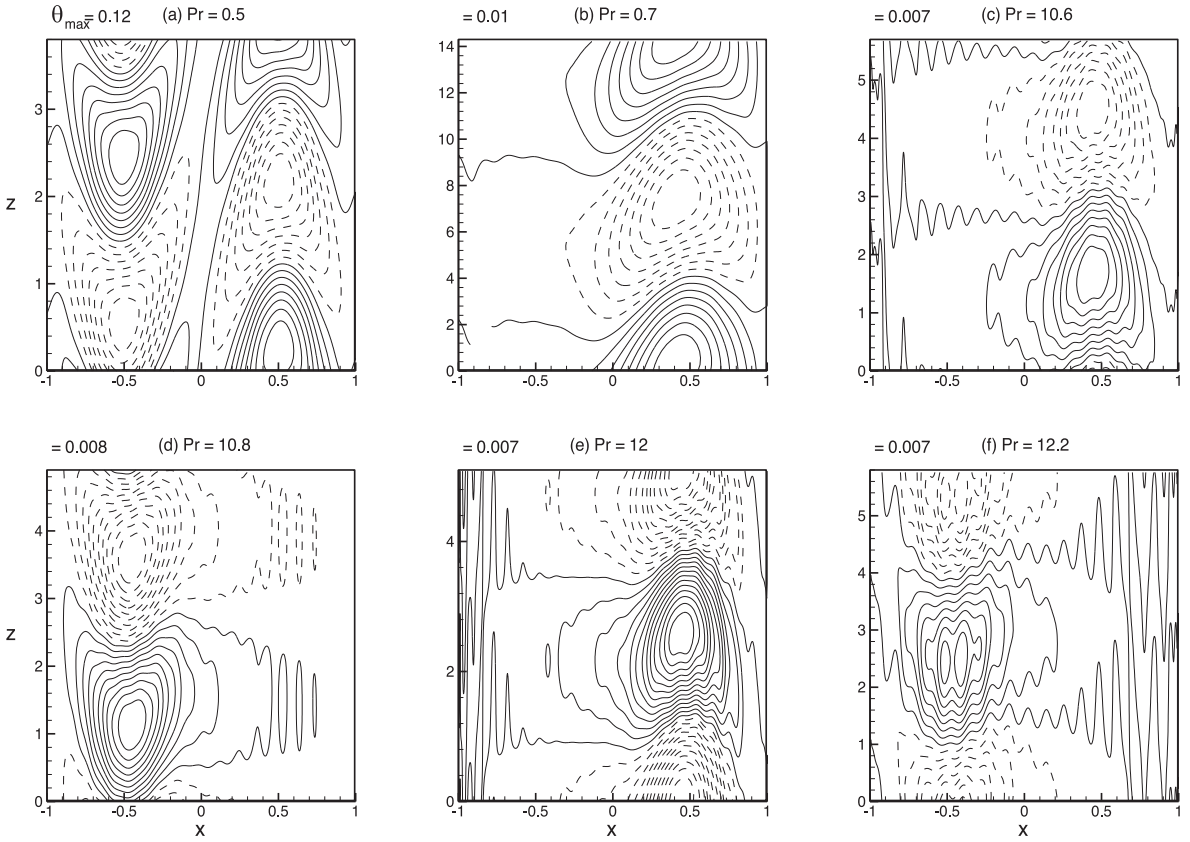

Fig. 11. Pattern variation of isotherms for different values of *Pr* when $\Lambda_c = 1$ and $R_{ea} = 500$.

method gives convergent results for $N=50$ in all the cases and the convergent results also differ as M increases. However, the results show up to 8 digit point accuracy for $M=1501$ and $N=50$. As M increased further to 1701 and N increased to 60 even then the results remain consistent. Hence, in all calculations M and N are fixed at 1501 and 50, respectively. Our numerical results are justified under some limiting cases. The eigenvalue of the most unstable mode computed for an isothermal channel flow in the absence of AC electric field and couple stresses by replacing *ia* with *iaRe* and taking $Pr = 1$ are tabulated in Table 2 for different N when $Re = 10,000$ and $a = 1$, and also the critical stability parameters are found to be $(R_{ec}, a_c) = (5772.25, 1.02)$. These results are in good agreement with those of Orszag [42]. A final check is made on the results obtained under the limiting case of $R_{ea} = 0 = 1/\Lambda_c$. For this case, the computed results reveal that the instability switches over from stationary mode to travelling-wave mode when the Prandtl number exceeds the value 12.7 (Table 3) and this result is in good agreement with the well established result in the literature (Korpela et al. [5], Bergholz [43]). The various tests provide a strong validation of our numerical results.

In the basic state, the AC electric field fails to influence the velocity field even in the presence of couple stresses. To the contrary, the presence of couple stresses influences the base flow and the same is evident from Fig. 2(a). In the figure, the results for ordinary dielectric fluids ($\Lambda_c \to \infty$) are also given through dotted curves as it facilitates to demarcate the effect of couple stresses clearly. The effect of increasing couple stress parameter Λ_c is to inhibit the base flow significantly. Fig. 2(b) and (c) respectively shows the effect of Prandtl number (*Pr*) and Grashof number (*G*) on the base flow. The basic velocity profiles are anti-symmetric about the vertical line at $x = 0$; however, they are not precisely centro-symmetric about $x = \pm 1/2$.

The triplets (G_c, a_c, c_c) are tabulated in Table 4 for a fixed value of $\Lambda_c(= 5)$ and for different values of R_{ea} and *Pr* ranging from 1 to 200 as it helps in knowing the mode of instability. Fascinatingly, the transition from stationary to travelling-wave instability occurs at $Pr = 7$ and this value remains invariant for all values of AC electric Rayleigh number. In other words, AC electric field shows no influence on the transition region. Nonetheless, the values of critical stability parameters vary with R_{ea}. The critical stability parameters are tabulated in Table 5 for a fixed value of $R_{ea}(= 500)$, and for different values of Λ_c and Prandtl number *Pr*. The value of *Pr* at which the transition from stationary to travelling-wave mode occurs is found to increase with increasing Λ_c. Besides, the critical Grashof number G_c at the transition mode decreases with increasing Λ_c and the value of *Pr* at which the transition mode occurs, approaches to that of non-polar fluids case as Λ_c increases. We

Table 1
Dependence of the most unstable eigenvalue on number of grid points as well as order of the base polynomials.

M	N	$G = 1000, R_{ea} = 200, Pr = 10, \Lambda_c = 5, a = 1.5$	
		c_r	c_i
701	20	−0.84455834	21.26577108
	30	−0.85454352	21.26586491
	40	−0.85449216	21.26572169
	50	−0.85449537	21.26572645
	60	−0.85449537	21.26572645
901	20	−0.84446213	21.26576909
	30	−0.85430723	21.26586532
	40	−0.85430652	21.26586107
	50	−0.85430651	21.26586241
	60	−0.85430651	21.26586241
1101	20	−0.84442912	21.26576810
	30	−0.85429974	21.26586325
	40	−0.85429982	21.26586420
	50	−0.85429983	21.26586611
	60	−0.85429983	21.26586611
1301	20	−0.84442402	21.26576799
	30	−0.85429973	21.26586930
	40	−0.85429990	21.26586611
	50	−0.85429992	21.26586614
	60	−0.85429994	21.26586614
1501	20	−0.84442402	21.26576799
	30	−0.85429973	21.26586930
	40	−0.85429992	21.26586612
	50	−0.85429993	21.26586614
	60	−0.85429994	21.26586614
1701	20	−0.84442402	21.26576799
	30	−0.85429973	21.26586930
	40	−0.85429992	21.26586612
	50	−0.85429993	21.26586614
	60	−0.85429994	21.26586614

Table 2
Computation showing the eigenvalue of the most unstable mode.

N	$Re = 10000, a = 1$
	c
05	0.52096345 + 0.00042109i
10	0.23796484 + 0.02476214i
15	0.23663728 + 0.00427730i
20	0.23725363 + 0.00371086i
25	0.23749570 + 0.00372889i
30	0.23749553 + 0.00372877i
35	0.23749553 + 0.00372878i
40	0.23749553 + 0.00372877i
50	0.23749553 + 0.00372877i

Table 3
Variation ofG_c, a_c and c_c as a function of Pr for $R_{ea} = 0 = 1/\Lambda_c$.

Pr	G_c	a_c	c_c
1.0	992.05636850	1.404	0
5.0	982.51616156	1.384	0
10.0	983.45694190	1.383	0
12.6	984.09135449	1.383	0
12.7	984.09135447	1.383	0
12.8	831.82237442	0.400	±24.83007732
13.0	769.99223337	0.420	±23.04185606
15.0	486.70350504	0.609	±14.69142616
20.0	301.16313195	0.823	±9.28312220

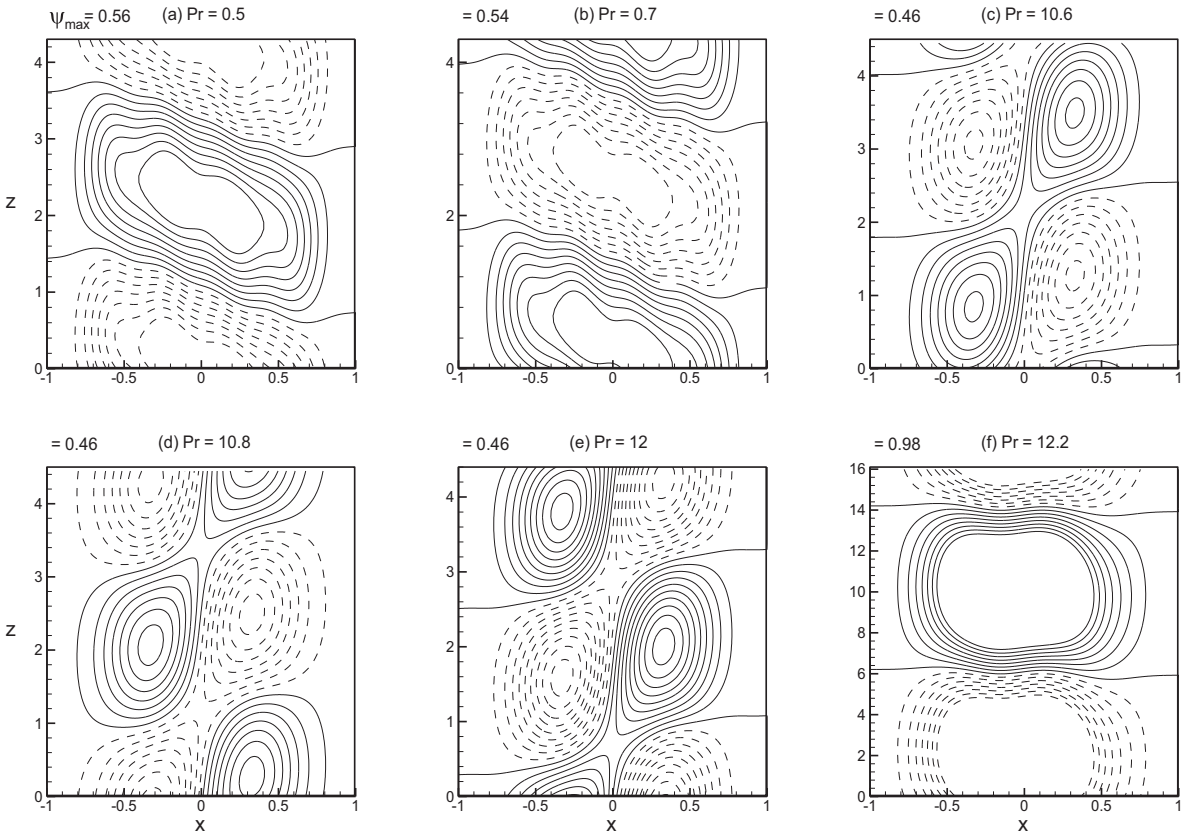

Fig. 12. Pattern variation of streamlines for different values of *Pr* when $\Lambda_c = 20$ and $R_{ea} = 500$.

also find that as *Pr* increases, c_c decreases for all values of R_{ea} and Λ_c considered, in a manner similar to that of maximum base velocity.

The neutral stability curves in the (*G*, *a*)-plane are displayed for various values of Prandtl number *Pr* in Fig. 3(a), (b) and (c) for $\Lambda_c = 5$, 10 and 20 respectively, when $R_{ea} = 500$. In Fig. 3(d) the neutral curves are presented for various values of R_{ea} when $Pr = 20$ and $\Lambda_c = 25$. It is observed that increase in R_{ea} and *Pr*leads to decrease in the region of stability as the portion below each neutral stability curve corresponds to stable region and above corresponds to instability.

Fig. 4(a) and (b) respectively shows the variation of G_c and the corresponding a_c as a function of *Pr* for different values of R_{ea} when $\Lambda_c = 5$. Till $Pr < 6.9$, the influence of *Pr* on G_c for a fixed value of R_{ea} is insignificant and exceeding which it is seen that G_c decreases suddenly (Fig. 4a). This is an indication that the buoyancy forces are the dominant source of instability at stationary mode. As observed in the Newtonian fluids case, the effect of increasing AC electric Rayleigh number is to instill instability but its influence is found to be very weak. Further, a_c decreases slowly with increasing *Pr* for a fixed value of R_{ea}, if the disturbances are stationary while an opposite behavior is noticed when the instability is via travelling wave mode (Fig. 4b). The critical wave number increases slightly with increasing R_{ea} and *Pr*. Another quantity of interest is c_c as it provides additional information about the nature of travelling-wave instability. Fig. 4(c) shows the variation of positive c_c with *Pr* for various values of R_{ea} and note that the variation of R_{ea} on c_c is found to be marginal. Also, c_c for the travelling-wave mode decreases monotonically with *Pr*. The discontinuity in c_c due to the transition from stationary to travelling-wave mode instability is shown by the vertical lines in the figure.

Both streamlines and isotherms at the critical state for stationary and travelling-wave modes are presented and analyzed in order to have a vivid picture on the stability behavior of the fluid flow. Figs. 5 and 6 show the results for different values of *Pr* at particular value of $R_{ea}(=200)$ and $\Lambda_c(=5)$. In the figures, dotted and solid lines represent negative and positive values, respectively. From Figs. 5(a) and 6(a), it can be seen that the flow pattern appears to be stationary cellular convection with an inclination in streamlines and isotherms respectively for $Pr = 1$. Further increase in *Pr* (= 5 and 6.8) results to force the convective motion to move closer and become parallel at the center of the vertical fluid layer (Fig. 5(b) and (c)), whereas shape of the isotherms changes from unicellular with an inclination, to bicellular oblate triangles which are occupying almost the whole thickness of vertical fluid layer (Fig. 6(b) and (c)). However, the strengths of secondary flow for the streamlines and isotherms do not vary much as a function of *Pr* in the stationary region. An abrupt change could be seen in stability profile as the instability mode changes from stationary to travelling-wave mode. Similarly, the flow pattern and

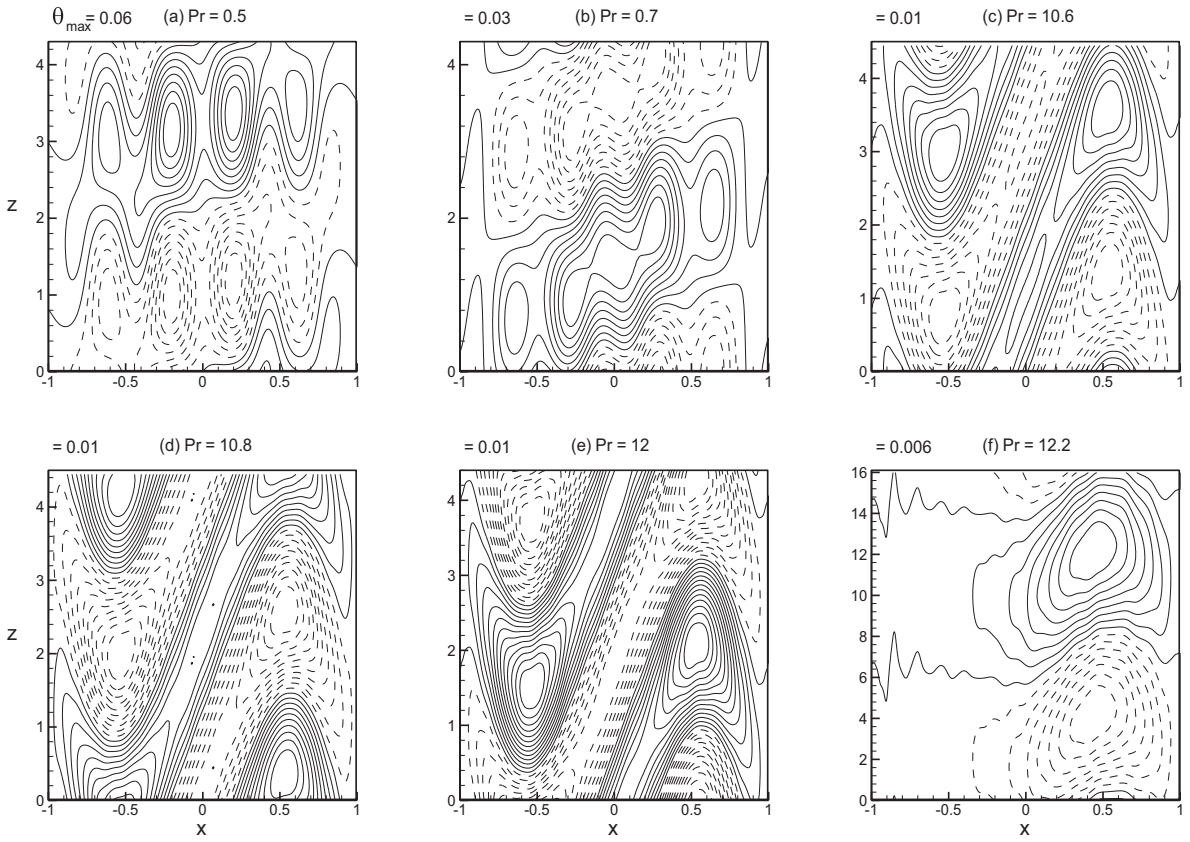

Fig. 13. Pattern variation of isotherms for different values of *Pr* when $\Lambda_c = 20$ and $R_{ea} = 500$.

flow strength change qualitatively as well as quantitatively as the mode changes from stationary to travelling-wave mode. In other words, the instability switches from stationary to travelling-wave mode, once the value of *Pr* exceeds the value 6.9. When ($Pr = 7$), convective cells transform into unicellular from bicellular in streamlines. Also, shape of the isotherms changes from bicellular oblate triangles to unicellular oblate triangles and concentrates in the vicinity of the hot wall. It is further seen that the actual wavelengths are substantially larger in both streamlines and isotherms and at this stage, $\psi_{\max}$ increases from 0.44 to 1.07. This fact is evident from Figs. 5(d) and 6(d). Further increase in *Pr* is seen to decrease the flow strength (Fig. 5(e) and (f)) and also to weaken the isotherms (Fig. 6(e) and (f)). When $Pr = 20$, convective cells change from unicellular to bicellular, and the magnitude of the flow strength decreases. The results presented for ($R_{ea} = 500$) and $\Lambda_c = 5$ are presented in Figs. 7 and 8 for different values of *Pr*. It is seen that change in the value of R_{ea} does not alter the pattern of streamlines and isotherms significantly, except for $Pr = 1$ (Figs. 7(a) and 8(a)) in which case a bicellular pattern is noticed in streamlines and oblate triangles in isotherms concentrating on the colder wall of the fluid layer.

To emphasize the effect of Λ_c on the stability aspects of the system, the variation of triplets (G_c, a_c, c_c) as a function of *Pr* is shown in Fig. 9 for a fixed value of $R_{ea} = 500$ and for different values of Λ_c. Fig. 9(a) shows the variation in G_c. In the figure, the results for ordinary dielectric fluids ($\Lambda_c \to \infty$) are also presented for the sake of comparison. Despite the presence of electric field, the results presented in the figure for different values of couple stress parameter are in accordance with those observed in its absence (Shankar et al. [35]). As is evident from the figure, the transition from stationary to travelling wave mode instability gets influenced by the presence of couple stresses noticeably**.** Moreover, it is observed that the presence of couple stresses increases considerably the threshold value of *Pr* at which the instability switches over from stationary to travelling-wave mode (Fig. 9(a))**.** In addition to the above observed facts, the figure also reveals that the effect of increasing Λ_c is destabilizing when the instability is occurring via stationary mode. Nonetheless, Λ_c shows a dual behavior on the stability of the system if the instability is via travelling-wave mode. The effect of *Pr* is found to be very weak if the instability is via stationary mode while its effect on the travelling-wave mode instability is somewhat observable. Fig. 9(b) exhibits the corresponding variation in a_c. As the instability takes over from stationary to travelling-wave mode, there exists a discontinuity in a_c and the vertical lines in the figure represent this behavior. Despite a_c depends strongly upon *Pr* at travelling-wave mode, the dependence of a_c upon *Pr* at stationary mode is seen to be marginal. Furthermore, a_c decreases with increasing Λ_c irrespective of the mode of instability. The results summarized in Fig. 9(c) for travelling-wave mode instability indeed confirm the above observed behavior more evidently. From the figure it is observed that c_c for the

Table 4
Variation of G_c, a_c and c_c as a function of R_{ea} and Pr for $\Lambda_c = 5$.

Λ_c	R_{ea}	Pr	G_c	a_c	c_c
5	0	1.0	1875.91610367	1.594	0
		5.0	1863.43688613	1.586	0
		6.0	1863.08291652	1.585	0
		6.9	1862.85656860	1.585	0
		7.0	1603.99342312	0.408	±34.20101078
		10.0	748.08560854	0.734	±16.35456603
		50.0	225.19644892	1.201	±5.28979261
		100.0	156.04107624	1.275	±3.72661112
		200.0	115.24019933	1.273	±2.79114372
	200	1.0	1854.68145108	1.595	0
		5.0	1859.02641511	1.586	0
		6.0	1859.35855603	1.589	0
		6.9	1859.66124183	1.586	0
		7.0	1595.09523755	0.408	±34.02039322
		10.0	742.11428149	0.740	±16.21185244
		50.0	219.70122552	1.161	±5.17368659
		100.0	156.98049760	1.241	±3.75715412
		200.0	114.47826123	1.278	±2.77158451
	500	1.0	1821.83648741	1.596	0
		5.0	1852.3684094	1.585	0
		6.0	1853.8133586	1.590	0
		6.9	1854.80584747	1.580	0
		7.0	1593.03301743	0.408	±33.96541328
		10.0	736.25648713	0.769	±16.01721295
		50.0	221.33534646	1.164	±5.20600240
		100.0	155.95606959	1.232	±3.73297067
		200.0	113.32131124	1.290	±2.74114488
	700	1.0	1799.21743853	1.596	0
		5.0	1847.88100368	1.583	0
		6.0	1850.13975298	1.585	0
		6.9	1851.58896616	1.582	0
		7.0	1590.57100661	0.408	±33.90780346
		10.0	727.30684972	0.771	±15.81774808
		50.0	214.81666698	1.198	±5.04246665
		100.0	150.88541156	1.280	±3.60507606
		200.0	112.53674722	1.281	±2.72321563

travelling-wave mode decreases with increasing Pr and Λ_c. The discontinuous changes in c_c are represented by the vertical lines which is due to the exchange of instability from stationary ($c_c = 0$) to travelling-wave ($c_c \neq 0$) mode.

The above observed facts are also viewed and analyzed through streamlines and isotherms. Figs. 10 and 11 exhibit streamlines and isotherms before and after the transition mode as a function of Pr for $\Lambda_c = 1$ and $R_{ea} = 500$. For $Pr = 0.5$, the secondary flow is bicellular. For a small change in the value of Pr from 0.5 to 0.7 there appears to be a sudden change in the magnitude of secondary flow (i.e.,$\psi_{\max} = 0.49$–1.19) and also the convective cell becomes unicellular. Besides, the magnitude of isotherms also found to reduce drastically ($\theta_{\max} = 0.12$–0.01) and variation in their pattern is also observed with the change in the mode of instability. Although the streamline and isotherm patterns remain the same with increasing Pr, the isotherms keep shifting from hot wall to cold wall of the fluid layer. The streamlines and isotherms are presented in Figs. 12(a) and (b) and 13(a) and (b) by changing only the value of Λ_c from 1 to 20 and keeping the other parametric values fixed as in Figs. 10 and 11 to know distinctly the impact of couple stress parameter on the flow behavior. The flow pattern appears to be stationary with streamlines tilted slightly, while isotherms, found to appear in multi-cellular convective cells. With increasing Pr(= 10.6, 10.8 and 12), the above observed pattern in streamlines and isotherms keeps changing from unicellular to bicellular in streamlines and also the magnitude of secondary flow becomes very weak. Fig. 12(c)–(e) confirm this behavior. As far as patterns in isotherms are concerned, multi-cellular cells become bicellular oblate triangles and this is evident from Fig. 13(c)–(e). At a higher value of Pr (=12.2), the flow strength suddenly changes both qualitatively and quantitatively in both streamlines and isotherms and this behavior is shown in Fig. 12(f) and (g).

6. Conclusions

The foregoing linear stability analysis reveals that the AC electric field has no influence on the basic velocity distribution while decrease in the couple stress parameter Λ_c inhibits the base flow. Although the effect of increasing R_{ea} is to instill instability on the system, the value of Pr at which the transition from stationary to travelling-wave mode instability occurs remains invariant for all values of R_{ea} even in the presence of couple stresses. The presence of couple stresses significantly alters the stability of the system. The effect of increasing Λ_c exerts destabilizing influence on the system at the stationary

Table 5
Variation of G_c, a_c and c_c as a function of Λ_c and Pr for $R_{ea} = 500$.

R_{ea}	Λ_c	Pr	G_c	a_c	c_c
500	∞	6.9	972.30957544	1.384	0
		7.0	972.48434818	1.386	0
		10.5	976.60323328	1.385	0
		10.6	976.67056119	1.385	0
		12.1	977.50544345	1.385	0
		12.2	977.56289190	1.385	0
		12.7	977.83238685	1.385	0
		12.8	818.55712926	0.400	±24.44426980
	5	6.9	1854.80585792	1.580	0
		7.0	1575.84713197	0.434	±33.43680108
		10.5	672.43982351	0.766	±14.77773388
		10.6	665.87645805	0.772	±14.63542005
		12.1	585.16560590	0.836	±12.93988817
		12.2	578.71422416	0.850	±12.38805097
		12.7	557.77223802	0.842	±12.38805097
		12.8	552.98801164	0.849	±12.28321903
	10	6.9	1109.86645019	1.481	0
		7.0	1110.01647508	1.482	0
		10.5	1113.12873161	1.484	0
		10.6	930.70670313	0.402	±25.42778237
		12.1	642.11283721	0.550	±17.66900430
		12.2	630.25808132	0.554	±17.36227428
		12.7	572.16551101	0.624	±15.74390209
		12.8	560.42991674	0.631	±15.43435057
	20	6.9	996.64834684	1.412	0
		7.0	996.82310617	1.414	0
		10.5	1000.64457452	1.413	0
		10.6	1000.71114151	1.413	0
		12.1	1001.47199577	1.415	0
		12.2	877.08808875	0.393	±25.57963051
		12.7	731.50591891	0.451	±21.42367962
		12.8	711.49686372	0.457	±20.86481544

mode and to the contrary it exhibits a dual behavior if the instability occurs via travelling-wave mode. The value of Pr, at which exchange of instability from stationary to travelling-wave mode takes place, increases with increasing Λ_c. The behavior of transition of instability is also viewed through the presentation of streamlines and isotherms before and after the change of mode of instability. A sudden change in streamlines and isotherms is observed both in their magnitude and pattern just before and after the transition mode and both bicellular as well as unicellular patterns of convective cells are observed for a wide of parameters.

Acknowledgments

One of the authors B.M.S. is indebted to Professor N. Rudraiah for his advice and encouragement and also wishes to thank the authorities of his University for their encouragement and support. The authors would like to extend their appreciation to the referees for their helpful comments to improve the quality of this article.

References

[1] K. Gotoh, M. Satoh, The stability of a natural convection between two parallel vertical planes, J. Phys. Soc. Jap. 21 (1966) 542–548.
[2] R.N. Rudakov, Spectrum of perturbations and stability of convective motion between vertical planes, Prikl. Mat. Mekh. 31 (1967) 349–355 (Appl. Math. Mech. 31 (1967) 376-383).
[3] K. Gotoh, N. Ikeda, Asymptotic solution of the instability problem of channel flows with antisymmetric velocity profile, J. Phys. Soc. Jap. 32 (1972) 845–850.
[4] R.V. Birikh, G.Z. Gershuni, E.M. Zhukhovitskii, R.N. Rudakov, On oscillatory instability of plane-parallel convective motion in a vertical channel, Prikl. Mat. Mekh. 36 (1972) 745–748 (Appl. Math. Mech. 36 (1972) 707-710).
[5] S.A. Korpela, D. Gozum, C.B. Baxi, On the stability of the conduction regime of natural convection in a vertical slot, Int. J. Heat Mass Transfer 16 (1973) 1683–1690.
[6] C.M. Vest, V.S. Arpaci, Stability of natural convection in a vertical slot, J. Fluid Mech. 36 (1969) 1–15.
[7] M. Takashima, The stability of natural convection in a vertical layer of electrically conducting fluid in the presence of a transverse magnetic fluid, Fluid Dyn. Res. 14 (1994) 121–134.
[8] A.O. El Moctar, N. Aubry, J. Batton, Electro-hydrodynamic micro-fluidic mixer, Lab Chip 3 (2003) 273–280.
[9] I. Glasgow, J. Batton, N. Aubry, Electroosmotic mixing in microchannels, Lab Chip 4 (2004) 558–562.
[10] H. Lin, B.D. Storey, M.H. Oddy, C.H. Chen, J.G. Santiago, Instability of electrokinetic microchannel flows with conductivity gradients, Phys. Fluids 16 (2004) 1922–1935.
[11] M.H. Oddy, J.G. Santiago, J.C. Mikkelsen, Electrokinetic instability micromixing, Anal. Chem. 73 (2001) 5822–5832.
[12] F.Q. Dang, L.H. Zhang, M. Jabasini, N. Kaji, Y. Baba, Characterization of electrophoretic behavior of sugar isomer by microchip electrophoresis coupled with videomicroscopy, Anal. Chem. 75 (2003) 2433–2439.

[13] J.J. Santos, B.D. Storey, Instability of electro-osmotic channel flow with streamwise conductivity gradients, Phys. Rev. E 78 (2008) 046316–046325.
[14] J.C. Baygents, F. Baldessari, Electrohydrodynamic instability in a thin fluid layer with an electrical conductivity gradient, Phys. Fluids 10 (1998) 301–311.
[15] H. Lin, Electrokinetic instability in microchannel flows: A review, Mech. Res. Commun. 36 (2009) 33–38.
[16] M. Takashima, H. Hamabata, The stability of natural convection in a vertical layer of dielectric fluid in the presence of a horizontal ac electric field, J. Phys. Soc. Jap. 53 (1984) 1728–1736.
[17] Y.M. Chen, A.J. Pearlstein, Stability of free-convection flows of variable viscosity fluids in vertical and inclined slots, J. Fluid Mech. 198 (1989) 513–541.
[18] K. Fujimura, Automated finder for the critical condition on the linear stability of fluid motions, JAERI-M 90-057, 1990.
[19] B.L. Smorodin, Stability of plane flow of a liquid dielectric in a transverse alternating electric field, Fluid Dyn. 36 (2001) 548–555.
[20] A.C. Ruo, M.H. Chang, F. Chen, Effect of rotation on the electrohydrodynamic instability of a fluid layer with an electrical conductivity gradient, Phys. Fluids 22 (2010) 024102-1-11.
[21] I.A. Frigaard, S.D. Howison, I.J. Sobey, On the stability of Poiseuille flow of a Bingham fluid, J. Fluid Mech. 263 (1994) 133–150.
[22] D. Gozum, V.S. Arpaci, Natural convection of viscoelastic fluids in a vertical slot, J. Fluid Mech. 64 (1974) 439–448.
[23] M. Takashima, The stability of natural convection in a vertical layer of viscoelastic liquid, Fluid Dyn. Res. 11 (1993) 139–152.
[24] A.C. Eringen, Theory of micropolar fluids, J. Math. Mech. 16 (1966) 1–18.
[25] V.K. Stokes, Couple stresses in fluids, Phys. Fluids 9 (1966) 1709–1715.
[26] M.S. Malashetty, S.N. Gaikwad, M. Swamy, An analytical study of linear and non-linear double diffusive convection with soret effect in couple stress liquids, Int. J. Therm. Sci. 45 (2006) 897–907.
[27] S.N. Gaikwad, M.S. Malashetty, K. Ramaprasad, An analytical study of linear and non-linear double diffusive convection with soret and Dufour effects in couple stress liquids, Int. J. Nonlinear Mech. 42 (2007) 903–913.
[28] M.S. Malashetty, I.S. Shivakumara, Sridhar Kulkarni, The onset of convection in a couple stress fluid saturated porous layer using a thermal non-equilibrium model, Phys. Lett. A 373 (2009) 781–790.
[29] Sunil, R. Devi, A. Mahajan, Global stability for thermal convection in a couple-stress fluid, Int. Commun. Heat Mass Transfer 38 (2011) 938–942.
[30] I.S. Shivakumara, S.B. Naveen Kumar, Linear and weakly nonlinear triple diffusive convection in a couple stress fluid layer, Int. J. Heat Mass Transfer 68 (2014) 542–533.
[31] I.S. Shivakumara, J. Lee, K. Vejravelu, M. Akkanagamma, Electrothermal convection in a rotating dielectric fluid layer: effect of velocity and temperature boundary conditions, Int. J. Heat Mass Trans. 55 (2012) 2984–2991.
[32] I.S. Shivakumara, M. Akkanagamma, C.O. Ng, Electrohydrodynamic instability of a rotating couple stress dielectric fluid layer, Int. J. Heat Mass Trans. 62 (2013) 761–771.
[33] J.K. Jain, V.K. Stokes, Effects of couple stresses on the stability of plane Poiseuille flow, Phys Fluids 15 (1972) 977–980.
[34] N. Rudraiah, B.M. Shankar, C.O. Ng, Electrohydrodynamic stability of couple stress fluid flow in a channel occupied by a porous medium, Spec. Top. Rev. Porous Med. 2 (2011) 11–22.
[35] B.M. Shankar, J. Kumar, I.S. Shivakumara, Stability of natural convection in a vertical couple stress fluid layer, Int. J. Heat Mass Transf. 78 (2014) 447–459.
[36] B.M. Shankar, J. Kumar, I.S. Shivakumara, Effect of horizontal alternating current electric field on the stability of natural convection in a dielectric fluid saturated vertical porous layer, J. Heat Transfer 137 (2015) 042501-1-9.
[37] L.D. Landau, E.M. Lifshitz, Electrodynamics of Continuous Media, Pergamon Press, 1960.
[38] P.G. Drazin, W.H. Reid, Hydrodynamic Stability, Cambridge University Press, Cambridge, UK, 2004.
[39] IMSL, International Mathematical and Statistical Library 1982.
[40] C.B. Moler, G.W. Stewart, An algorithm for generalized matrix eigenvalue problems, SIAM (Soc. Ind. Appl. Math.) J. Numer. Anal. 10 (1973) 241–256.
[41] B.M. Shankar, J. Kumar, I.S. Shivakumara, C.O. Ng, Stability of fluid flow in a Brinkman porous medium—a numerical study, J. Hydrodynamics 26 (2014) 681–688.
[42] S.A. Orszag, Accurate solution of the Orr-Sommerfeld stability equation, J. Fluid Mech. 50 (1971) 689–703.
[43] R.F. Bergholz, Instability of steady natural convection in a vertical fluid layer, J. Fluid Mech. 84 (1978) 743–768.